Development of the Heating Scenarios to Achieve High-Ion Temperature Plasma in the Large Helical Device*)

Yasuhiko TAKEIRI[1,2], Osamu KANEKO[1,2], Masaki OSAKABE[1], Kenichi NAGAOKA[1,2], Sadayoshi MURAKAMI[3], Hiromi TAKAHASHI[1], Haruhisa NAKANO[1], Katsumi IDA[1,2], Shigeru MORITA[1,2], Masayuki YOKOYAMA[1], Mikiro YOSHINUMA[1,2], Keisuke FUJII[4], Motoshi GOTO[1,2], Chihiro SUZUKI[1], Ryosuke SEKI[1], Katsuyoshi TSUMORI[1,2], Katsunori IKEDA[1], Masashi KISAKI[1], Takashi MUTOH[1,2], Hiroshi YAMADA[1,2], Akio KOMORI[1,2] and the LHD Experiment Group

[1] *National Institute for Fusion Science, Toki 509-5292, Japan*
[2] *The Graduate University for Advanced Studies, Hayama, Kanagawa 240-0193, Japan*
[3] *Department of Nuclear Engineering, Kyoto University, Kyoto 615-8530, Japan*
[4] *Department of Mechanical Engineering and Science, Kyoto University, Kyoto 615-8540, Japan*

(Received 6 February 2014 / Accepted 4 October 2014)

High-ion temperature experiments in the Large Helical Device (LHD) are categorized in terms of the heating scenarios that are closely related to the development of neutral beam injection (NBI) systems. Although high-energy tangential negative-NBI heating has greatly contributed to extending the plasma parameter regime in LHD, the ion temperature does not increase because the electron heating is dominant with negative-NBIs. In the high-Z discharges, it was demonstrated that the ion temperature increased with an increasing ion heating power and achieved 13.5 keV with the negative-NBIs. Low-energy perpendicular positive-NBIs were installed for the ion heating, and the ion temperature was increased to more than 7 keV in hydrogen discharges. In the high-ion temperature plasmas, an ion internal transport barrier (ion ITB) was formed, and the impurity hole was observed in the core. Long-pulse ion cyclotron range of frequency heating (ICH)/electron cyclotron resonance heating (ECRH) helium discharges are effective for wall conditioning, leading to a decrease in the neutral density and a peaked density profile. Consequently, the ion heating efficiency increases in the core, and the central T_i is raised up to 7.5 keV. With the superposition of high-power ECRH, high-performance plasmas of $T_i \sim T_e \sim 6$ keV were obtained. In the planned deuterium experiment, the ion heating power will be increased with the deuterium beam injection, and $T_i = 10$ keV is expected.

Keywords: high-ion temperature plasma, Large Helical Device, NBI heating, high-Z discharge, ion ITB, impurity hole, long-pulse discharge cleaning, deuterium experiment, ion and electron root

DOI: 10.1585/pfr.10.1402001

1. Introduction

The Large Helical Device (LHD), which is the world's largest superconducting helical device, became operational in 1998 for the reactor-relevant helical plasma research [1–3]. The steady-state operation of high-temperature and high-density plasmas is required in a fusion reactor, and, to date, LHD has significantly contributed to the establishment of the scientific basis of a helical reactors by offering the advantage of the steady-state operation [1–7]. In the design phase of LHD, neutral beam injection (NBI) heating with tangential injection was selected as the main heating method because perpendicular fast ion confinement had not been fully understood at that time. Since high-injection energy of 180 keV for hydrogen beams is required for effective plasma heating with the tangential injection, the negative-ion-based NBI (negative-NBI) system, which had not been in practical use at that time, was developed and installed in LHD [8–12]. The tangential high-energy negative-NBI has greatly contributed to the high-performance plasma production and extension of the LHD parameter regime, especially for high-density and high-β plasmas [3–5]. However, the ion temperature did not increase with the negative-NBI because such high-energy ions mainly heat electrons. After confirming the effectiveness of ion heating in high-Z discharges and the confinement of perpendicularly accelerated ions in the ion cyclotron range of frequency heating (ICH) experiments, a low-energy perpendicular positive-ion-based NBI (positive-NBI) system was installed in LHD [4, 13, 14]. With high-power plasma heating using the positive-NBI, the ion temperature was significantly raised, and the central ion temperature of 7 keV was achieved by combining negative- and positive-NBIs [6, 15].

author's e-mail: takeiri@nifs.ac.jp

*) This article is based on the invited talk at the 30th JSPF Annual Meeting (2013, Tokyo).

In this study, we discuss the progress of the high-T_i experiments in LHD and focus on the heating scenarios based on the NBI development. Furthermore, we present the achievements of extending the ion temperature regime up to 7.5 keV and the integration of high-ion and high-electron temperature plasmas, and discuss the deuterium experiment.

2. Neutral Beam Injection Systems in LHD

LHD is equipped with three negative-ion-based neutral beam (NB) injectors and two positive-ion-based NB injectors, as shown in Fig. 1. After intensive development of the negative-NBI system for 8 years [8–10], two negative-NB injectors of BL1 and BL2 were constructed and became operational in 1998, as one of the first operational negative-NBI systems in the world [1, 12]. A third negative-NB injector (BL3) became operational in 2001 [11]. High-energy hydrogen beams of 180 keV are tangentially injected, and the design injection power is 5 MW in an injector. The injection power of tangential negative-NBIs has been steadily increasing because of continuous improvements, and a total injection power of 16 MW is achieved with the three injectors, exceeding the designed value of 15 MW [14, 16], which has contributed to the achievement of high plasma performance in LHD.

The high-energy particles accelerated by ICH were effectively confined [17], and an ion tail up to 2.5 MeV was observed in inward-shifted configurations of the magnetic axis [18]. In addition, in full-orbit calculations, a significant loss of the high-energy ions was not observed [19]. Based on the successful ICH heating results, perpendicularly injected NBI heating is considered possible in inward-shifted configurations. Thus, to increase the ion heating power, low-energy positive-NBI systems with perpendicular injection were proposed and projected.

Two positive-NBI systems, BL4 and BL5, with low injection energy of 40 keV were installed in 2005 and 2010, respectively. A positive-NB injector has four positive ion sources, and the world's largest positive ion source was developed to achieve an injection power of 6 MW at 40 keV [14]. Consequently, the injection power of 12 MW was achieved with two injectors. The BL4 is also used in ion temperature profile measurement with charge exchange spectroscopy (CXS) [20]. The highly reliable LHD-NBI system is operated as a primary heating device in order to extend the LHD parameter regime.

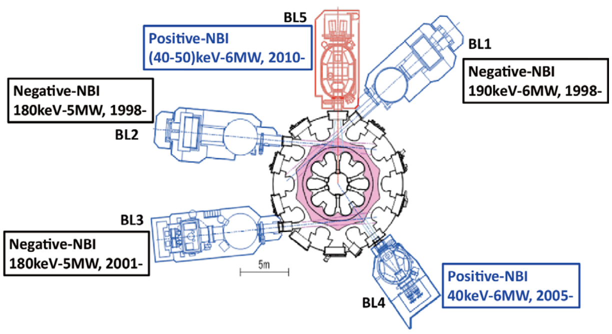

Fig. 1 Plan view of the NB injectors installed in LHD. The three negative-NB injectors of BL1, BL2 and BL3 are arranged for the tangential injection, and the two positive-NB injectors of BL4 and BL5 are arranged for the perpendicular injection.

3. High-T_i Experiments in the Design Phase of LHD

In designing the LHD, the confinement of fast ions, especially the perpendicularly accelerated ions, was not well confirmed. Thus, the high-energy tangential negative-NBI heating was selected as the main approach to achieve high-performance plasmas. To produce high-$n\tau T$ plasmas at the target density of $(3 - 5) \times 10^{19}\ \mathrm{m}^{-3}$, the injection energy of hydrogen beams was determined as 180 keV. However, for high-T_i experiments for lower density plasmas, the injection energy is too high to effectively heat the ions. In order to obtain high-T_i plasmas, the neoclassical electron root scenario, in which the ion transport is much improved with the generation of a positive radial electric field, was adopted by adding high-power ECRH [21–23].

Although the negative-NBI heating successfully extended the LHD parameter regime for high-$n\tau T$, high-density, and high-β plasmas, the achieved ion temperature was less than 2 - 3 keV in hydrogen discharges because the ion heating power is not sufficient to increase the ion temperature in low density plasmas [24, 25]. Owing to the high injection energy, a large fraction of the injected neutral beam passes through low-density plasmas without ionization, and most of the ionized beam power heats the electrons. High-electron temperature plasmas have been achieved with centrally focused ECRH; furthermore, improvement in the electron confinement was observed owing to the suppression of the anomalous transport in the electron internal transport barrier (ITB) plasmas formed in the electron root [26, 27]. However, the electron root scenario for increasing the ion temperature has not been confirmed, mainly because of the shortage in the ECRH power and ion heating power.

4. High-T_i Plasmas Achieved by High-Z Discharges with Negative-NBIs

In the initial phase of the LHD project, a large fraction of the heating power was transferred to the electrons owing to the high beam energy with the negative-NBIs. Then, high-Z discharges were proposed to increase the ion heating power normalized by the ion density (P_i/n_i) and investigate the capability of high-T_i plasma confinement in LHD. The ionization rate of the injected neutral beam was increased in high-Z plasmas, and the absorption power was much enhanced in low-density plasmas injected with high-energy beams. In addition, the direct ion heating power increased owing to the reduced number of ions in the high-Z plasmas, compared with the same electron-density plasmas in hydrogen discharges.

Glow discharge cleaning with neon (Ne) / argon (Ar) gas is effectively minimizes the wall-absorbed hydrogen with which the high-Z plasma would be diluted during the discharge. Heavier gas species such as Ar are more effective to realize high-Z discharges at lower ion density owing to the higher charge number. After the intensive Ne or Ar glow discharge cleaning, high-Z plasmas were successfully produced at low densities with Ar gas puff [25].

Figure 2 shows the time evolution of injection and absorption power of the negative-NBI, the line-averaged electron density measured with a far-infrared (FIR) interferometer, and the central ion temperature measured with the Doppler broadening of an X-ray of Ar XVII line in an Ar-puffed plasma after the Ar glow discharge cleaning [28]. After increasing the electron density owing to the Ar gas puff at $t = 0.5$ s, the central ion temperature rapidly increases during density reduction with another injection of NBI power and reaches 13.5 keV. The central electron temperature (not shown) is around 4.2 keV with Thomson scattering, which is much lower than the ion temperature. The appropriate range of the electron density is $0.3 - 0.4 \times 10^{19}$ m^{-3} for high-T_i, and the decay time of the ion and electron temperatures is extremely long after the beam-off.

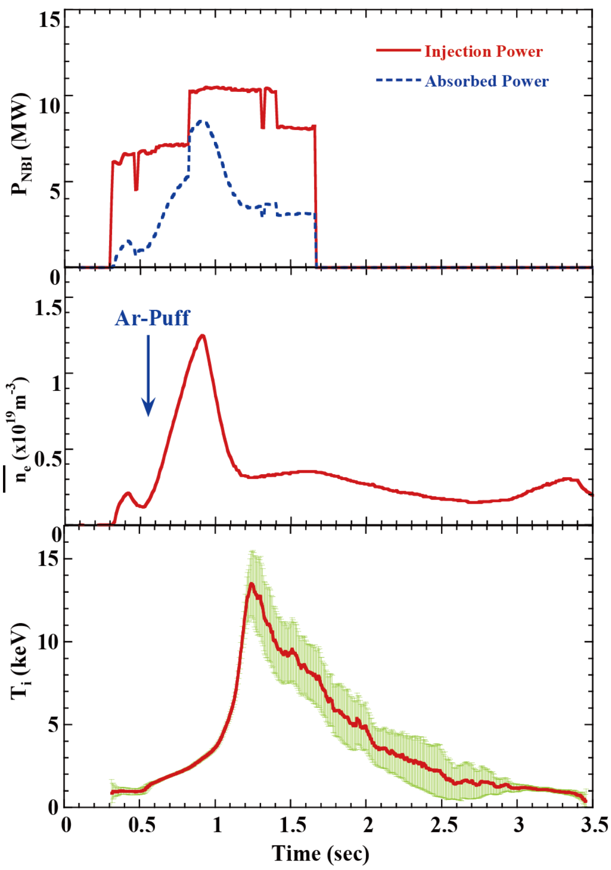

Fig. 2 Time evolutions of the injection and the absorbed powers of the negative-NBIs, the line-averaged electron density measured with the FIR interferometer, and the central ion temperature measured with the Doppler broadening of an X-ray line of ArXVII in an Ar-puffed plasma after the Ar-glow discharge cleaning. The Ar gas is briefly puffed at $t = 0.5$ s. (from ref. [28])

In high-Z plasmas, the hydrogen ion density is roughly estimated at 25% - 40% of the electron density, and the H ions dominate the species number ratio even in the high-Z plasmas. $Z_{\rm eff}$ is in the range of 7 - 12, and the total ion density should be 30% - 46% of the electron density [25]. Then, the ion heating power normalized by the ion density can be estimated, and the ion temperature depending on it is shown in Fig. 3 for the Ar- and Ne-puffed plasmas after Ne-glow discharge cleaning [25]. The ion temperature is increased by increasing the density-normalized ion heating power, and no distinct saturation in the ion temperature is observed. The anomalous transport causing the power degradation of the ion temperature would be suppressed in high-T_i plasmas obtained in the high-Z discharge. In hydrogen discharges, the density-normalized ion heating power was limited to 2 - 3 MW/10^{19} m^{-3}, thus T_i was below 2 - 3 keV. The results in the high-Z discharges suggest that a high-ion temperature as well as hydrogen discharges will be achieved if the direct ion heating power is increased [28, 29].

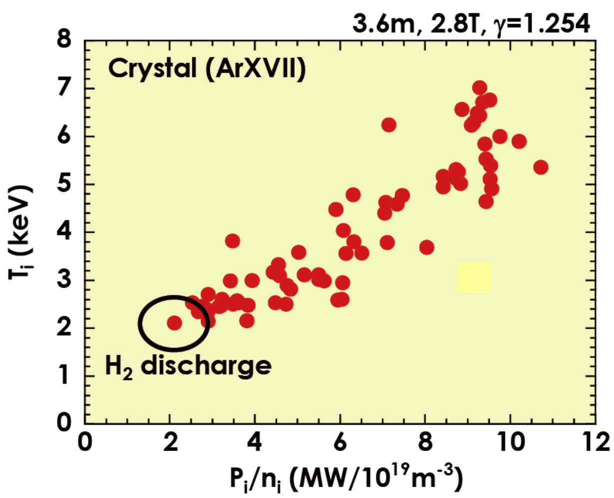

Fig. 3 Central ion temperature as a function of the ion heating power normalized by the ion density in the high-Z plasmas heated by negative-NBIs. The range of the density-normalized ion heating power is also shown in the hydrogen discharges together with the achieved ion temperature. (from ref. [25])

5. High-T_i Plasmas Achieved by Adding Positive-NBI

5.1 Ion ITB formation by carbon pellet injection

To increase the ion heating power, two positive-NB injectors, BL4 and BL5, were installed at LHD, and became operational in 2005 and in 2010, respectively [13, 14]. High-ion temperature plasmas greater than 7 keV have been realized by enhancing the ion heating power [30]. Figure 4 shows the central ion temperature measured with the CXS as a function of the electron-density-normalized ion heating power. By increasing the ion heating power with the development of low-energy positive-NB injectors, the ion temperature increased in 2009 and 2010, as shown in Fig. 4. In 2011 and 2012, the density-normalized ion heating power was increased by using the wall conditioning scheme, leading to further increases in the ion temperature [31], discussed in Sec. 5.3. Z_{eff} was roughly estimated at 1.5 - 2.5 for these plasmas, and it should be noted that the dependency of the ion temperature on the ion-density-normalized ion heating power is similar to that observed in the high-Z plasmas shown in Fig. 3.

The high-T_i plasmas that are realized with positive- and negative-NBIs are characterized by the formation of ion ITB. Figure 5 (a) shows the time evolution of the plasma parameters in an ion ITB plasma formed with a carbon pellet injection. A carbon pellet, 1 mm in diameter and 1 mm in length, is injected at t = 4.56 s, and, subsequently, the electron density is increased stepwise. The ion temperature increases in the density decay phase after the carbon pellet injection and reaches 7.5 keV with the ion ITB formation, as shown in Fig. 5 (b). Subsequently, the ion temperature decreases, showing back transition to normal confinement. Contrarily, the electron temperature is

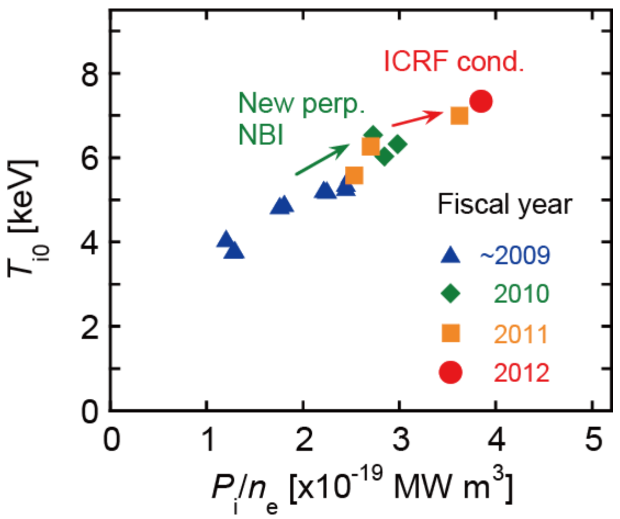

Fig. 4 Central ion temperature measured with charge exchange spectroscopy (CXS) as a function of the electron-density-normalized ion heating power in the low-Z discharges after the installation of the positive-NBIs (low-energy and perpendicular injection). The density-normalized ion heating power increased with the development of positive-NBIs in 2009 and 2010 and with progress of the wall conditioning in 2011 and 2012.

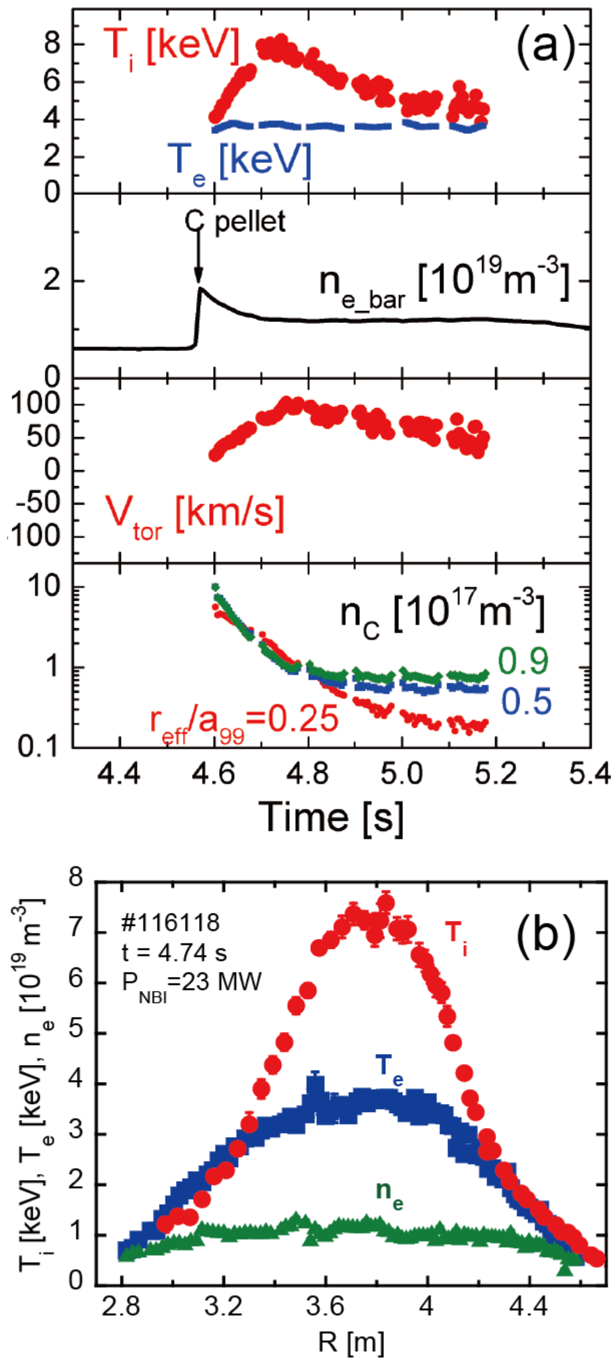

Fig. 5 (a) Time evolution of the central ion and electron temperatures, the line-averaged electron density, the toroidal rotation velocity, and carbon density at r_{eff}/a_{99} = 0.25, 0.5 and 0.9 in the ion ITB plasma formed with a carbon pellet injection. (b) Profiles of the ion and the electron temperatures and the electron density at t = 4.74 s in the ion ITB plasma. The port-through power of negative- and positive-NBIs are 13.7 MW and 9.3 MW, respectively.

almost constant during the ion ITB formation. The toroidal rotation in the core is enhanced corresponding to the rise in the ion temperature. Carbon density rapidly decreases with increasing ion temperature, and the outward convection of the carbon impurity is maintained during the decrease in the ion temperature after the back transition.

The transport analysis was performed for the ion ITB plasma formed with the carbon pellet injection by using the TASK3D-a02 transport analysis suite [32], which is applicable to significantly time-evolved plasmas such as pellet injection. Figure 6 (a) shows that after the carbon pellet injection at $t = 4.56$ s, the ion temperature gradient becomes steep in the core and ion ITB forms as the ion temperature increases. Correspondingly, the thermal diffusivity in the core decreases to the neoclassical level owing to the significant reduction of the anomalous transport, as shown in Fig. 6 (b), which shows the ion thermal diffusivity normalized by the 3/2 power of the ion temperature as the anomalous transport factor. In heavy ion beam probe (HIBP) measurements, the high-T_i plasma shows negative radial electric field (E_r) in the core that is consistent with the neoclassical prediction, and the transition of the radial electric field has not been observed in the ion ITB formation [33–35]. Thus, the ion ITB is attributed to the reduction of the anomalous transport in the ion root with negative E_r.

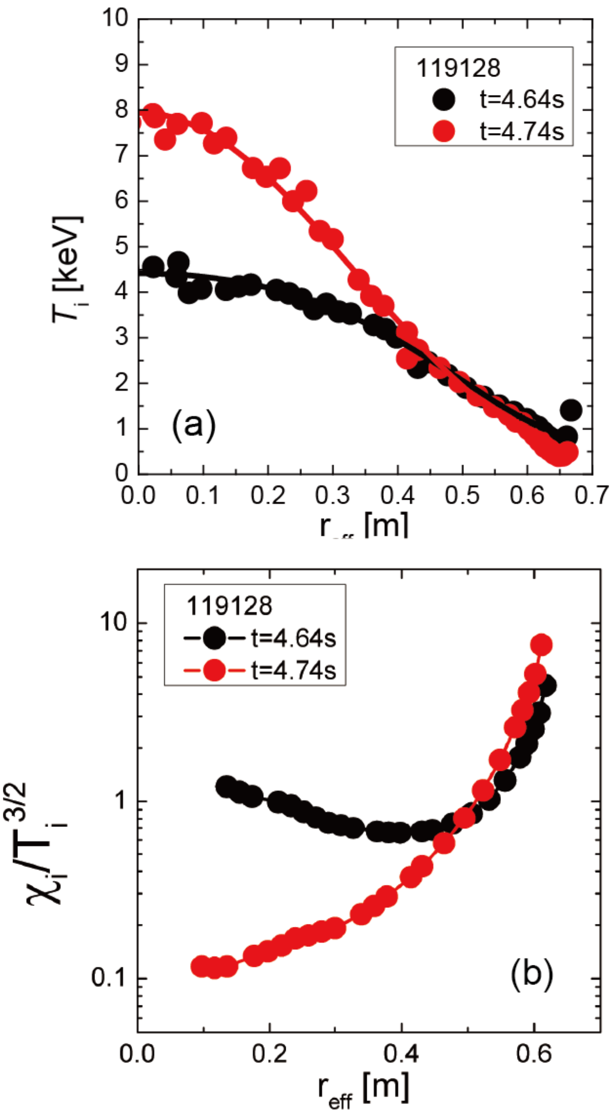

Fig. 6 (a) Ion temperature profiles before ($t = 4.64$ s) and after ($t = 4.74$ s) the ion ITB formation. The carbon pellet is injected at $t = 4.56$ s. (b) Ion thermal diffusivity normalized by the 3/2 power of the ion temperature as the anomalous transport factor before and after the ion ITB formation indicated in (a). The transport analysis is performed with the TASK3D-a02 transport analysis suite [32]. The port-through power of the negative- and positive-NBIs is 14.1 MW and 10.0 MW, respectively.

High ion temperature plasma with ion ITB formation is also observed without the carbon pellet injection. The ion temperature of around 6 keV is maintained with helium (He) gas puffing, and the heat transport property in the steady state ion ITB plasma is almost the same as that in the ITB plasma with the carbon pellet injection [36].

5.2 Formation of impurity hole

One of the distinguishing features in high-T_i plasmas is the formation of impurity hole [37, 38]. As explained in Fig. 5 (a), the carbon density rapidly decreases with ion ITB formation. Figure 7 (b) shows the time evolutions of the radial profile of the CVI emission intensity in high-T_i discharge with the carbon pellet injection shown in Fig. 7 (a) [39]. The carbon emission intensity decreases as the ion temperature increases, and the reduction in the carbon emission intensity is stronger in the inner regions, leading to the formation of impurity hole in the core. The carbon density in the core continues to decrease even in the decreasing phase of the ion temperature, forming an extremely hollow impurity profile. Figure 7 (c) shows the Ne and He density profiles in the impurity holes. These impurities also show hollow profiles in the ion ITB plasma; nonetheless, the stronger impurity hole was observed for the heavier impurities [39]. Impurity hole formation is desired in a reactor because the impurity accumulation should be suppressed in a burning plasma.

5.3 Effect of wall conditioning on high-T_i plasmas

Wall conditioning strongly affects high-T_i plasmas. Higher ion temperature plasma is realized with low recycling conditions. Repetitive long-pulse ICH helium main discharges are applied to wall conditioning for decreasing the residual hydrogen [40]. Figure 8 (a) shows the time variation in the partial pressure of residual hydrogen during a series of the experiments. The residual hydrogen partial pressure gradually increases during successive main discharges in the high-T_i experiments, resulting in deterioration of the achieved ion temperature. Then, long-pulse

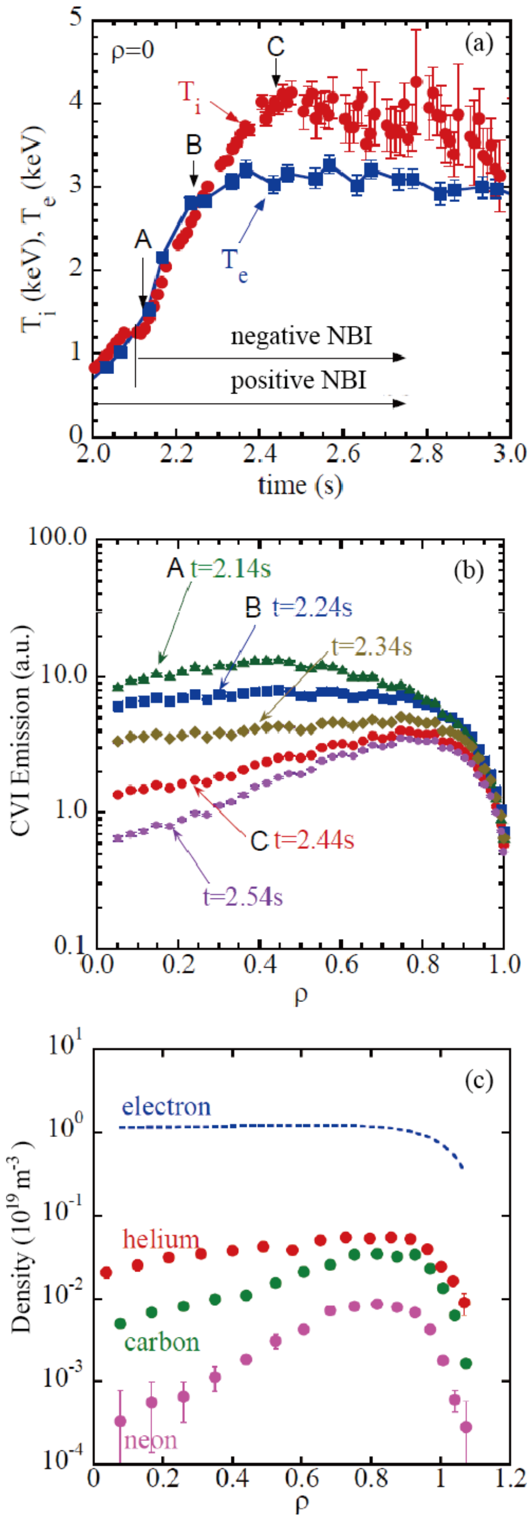

Fig. 7 (a) Time evolution of the central ion and electron temperatures in the ion ITB plasma with the carbon pellet injection. (b) Time variation of the radial profile of the CVI emission intensity for the plasma shown in (a). (c) Radial profiles of the helium, carbon and neon densities in the plasma forming the impurity hole. The electron density profile is also indicated by the dotted line as a reference. (from ref. [39])

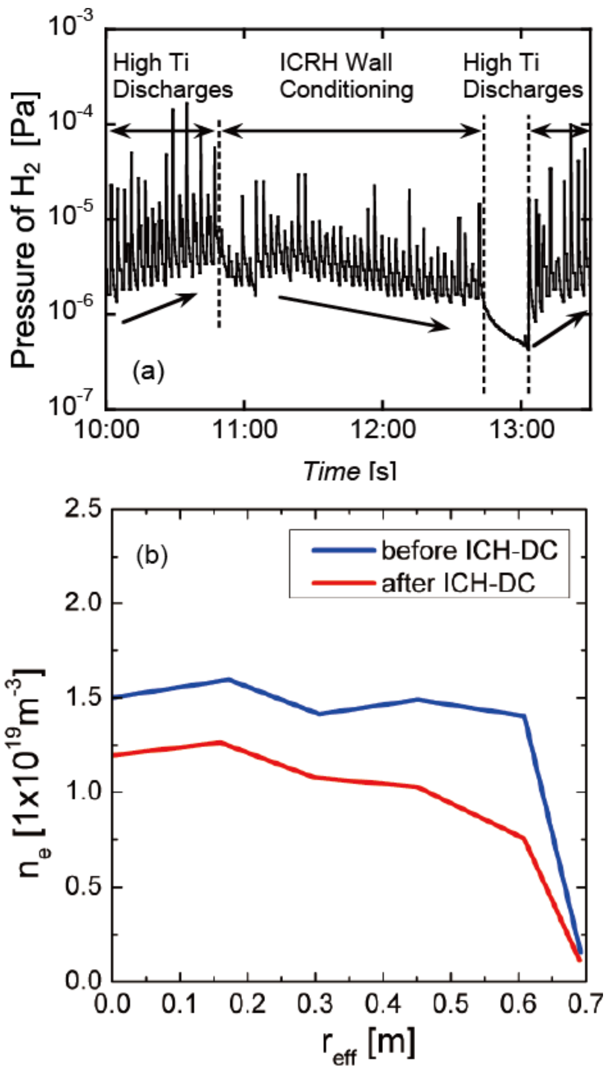

Fig. 8 (a) Time variation of the partial pressure of residual hydrogen during the high-T_i experiments and ICH long-pulse discharges for wall conditioning. (b) Electron density profiles before and after wall conditioning with ICH main discharges.

ICH helium main discharges for 10 sec were repeated, and the residual hydrogen pressure was decreased shot by shot. The reduction in residual hydrogen pressure confirmed in the repetitive ECRH long-pulse discharges for wall conditioning. After wall conditioning with the long-pulse helium main discharges, the density profile had more peaks as the edge pedestal weakened, as shown in Fig. 8 (b). As a result, the ion heating power ratio inside the half-radius increased by 15%, and the ion heating efficiency in the core improved, leading to increased peak ion heating profile [31].

The long-pulse ICH conditioning reduced the hydrogen neutral density in the core. The density profile of the neutral particles is measured with a high-dynamic range of Balmer-α spectroscopy [41]. The reduction in the neutral particle density from 3×10^{13} m^{-3} to 1.6×10^{13} m^{-3}

was observed even in the core after the conditioning discharges where the ion density is assumed to be identical to the electron density. An increase in the neutral density was not observed during the high-T_i discharge. Then, the charge-exchange loss of fast ions was maintained at a low level and did not seem to correlate with the back transition from the ion ITB. The ratio of the charge-exchange loss power to the ion heating power was evaluated for plasmas before and after the conditioning discharges. It was thus confirmed that the ratio reduced from 14% before the conditioning to 7% after the conditioning. The charge-exchange loss of fast ions is mainly dominated in the low energy range, which corresponds to the injection energy of the positive-NBI. Therefore, the decrease in the neutral density by the conditioning discharges enhances the ion heating power [31].

Owing to the peaking of the density profile and the decrease in the charge-exchange loss of fast ions after the conditioning main discharges, the ion heating power increased. Figures 9 (a) and (b) show the time evolution of the ion temperature and electron density, respectively, for high-T_i plasmas with the carbon pellet injection before and after wall conditioning by ICH helium main discharges. By decreasing the wall recycling with the conditioning discharges, the central ion temperature increased from 5 keV to around 7.5 keV with decreased density. Figure 9 (c) shows the ion heat flux as a function of the ion temperature gradient before and after wall conditioning by ICH helium main discharges [31]. The ion heat flux enhances owing to the increase in the ion heating power and the decrease in the density after the conditioning main discharges. As shown in Fig. 9 (c), in the low heat flux region, which is the same as that before the conditioning discharges, the heat transport properties after the conditioning discharges are identical to those before the conditioning discharges, and the T_i-gradient increases with increasing heat flux.

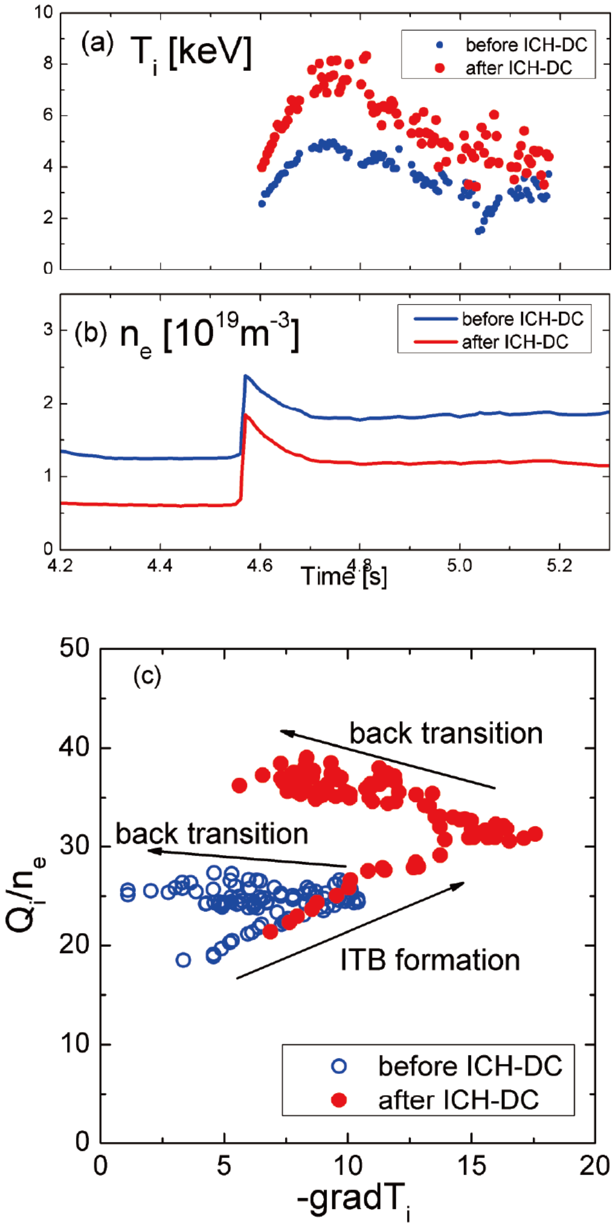

Fig. 9 Time evolution of (a) the ion temperatures and (b) the electron density for high-T_i shots with carbon pellet injection before and after the wall conditioning with ICH main discharges. (c) Ion heat flux as a function of the ion temperature gradient at $r_{eff}/a_{99} \sim 0.5$ before and after the wall conditioning with ICH main discharges [31]. The ion heat flux was estimated by considering the charge exchange loss. The port-through power of negative- and positive-NBIs are respectively 13.9 MW and 8.8 MW for the discharge before the ICH conditioning and 14.1 MW and 10.0 MW for the discharge after the ICH conditioning.

5.4 Increasing T_e in high-T_i plasma

The electron temperature in the NBI-heated ion ITB plasma is not sufficiently high, being lower than 4 keV, compared with the ion temperature. To extend the temperature regime, the ECRH was superposed to the ion ITB plasma. Figure 10 (a) shows the ion and the electron temperature profiles in the ion ITB plasma superposed by the ECRH. The electron density profile is also shown in the figure. The central electron temperature increased by superposing the ECRH, and peaked temperature profiles were observed for both the ions and the electrons. Consequently, high performance plasmas with 6 keV in both the ion and the electron temperatures were achieved after the wall conditioning by helium main discharges. By simultaneously achieving high ion and electron temperatures, the operational space for high temperature plasmas is extended, as shown in Fig. 10 (b), which indicates that the electron temperature in ion ITB plasmas is increased by the superposition of the ECRH. Further investigations will develop scenarios towards the reactor relevant plasma production.

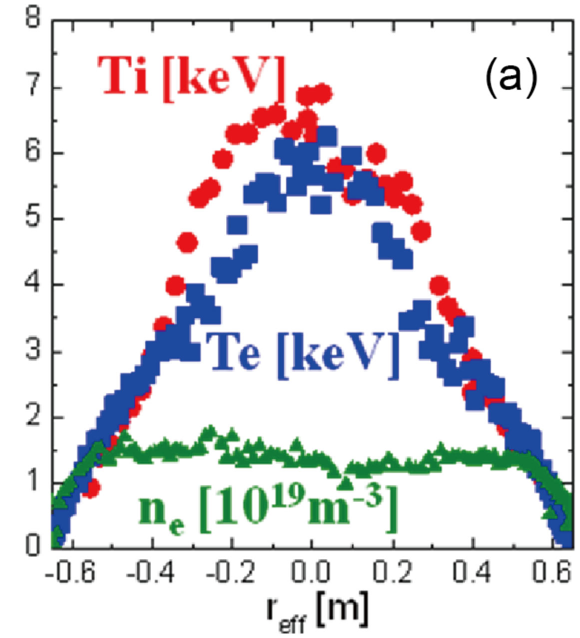

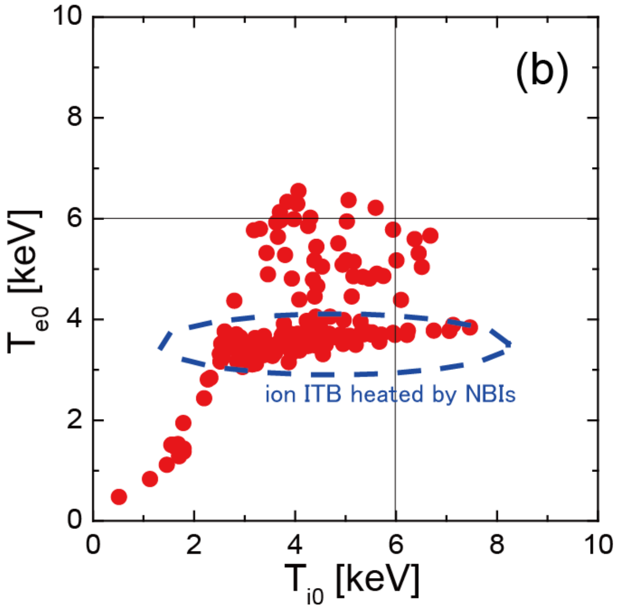

Fig. 10 (a) Ion and the electron temperature profiles in the ion ITB plasma superposed by the ECRH. The electron density profile is also shown. The port-through power of negative- and positive-NBIs is 15.1 MW and 10.4 MW, respectively. (b) Operational space of the electron and ion temperatures for the ion ITB plasmas heated by NBIs only and those superposed by ECRH.

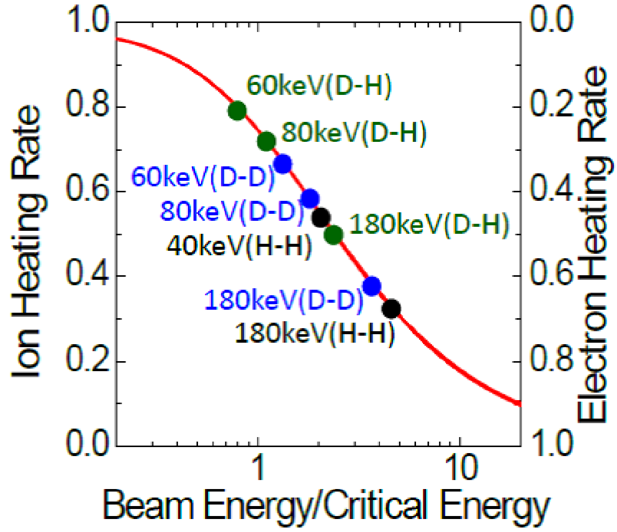

Fig. 11 Ion and electron heating rates for various combinations of the target plasma and beam species in the present hydrogen NBI systems and planned deuterium NBI systems.

6. Prospect for High-T_i Deuterium Plasma

The deuterium experiment is the next project in LHD [42]. The objectives of the LHD deuterium experiment for realizing high-performance plasmas relevant to the reactor by improving confinement and studying the mass dependence (isotope effect) in plasma confinement are summarized. For the high-T_i plasma experiments, the operational temperature regime is expected to increase owing to the increase in the ion heating power and the optimization of the discharge scenario.

The two positive-NBI systems with perpendicular injection will be upgraded for the deuterium beam operation to 9 MW from 6 MW by raising the injection energy from 40 keV to 60 keV in BL4 and to 80 keV in BL5. Consequently, the ion heating power should be enhanced. On the other hand, the three high-energy negative-NBI systems with tangential injection will remain unchanged with injection energy of 180 keV even for deuterium beams. A deuterium beam injection power of 32 MW is planned (18 MW and 14 MW in the positive- and the negative-NBIs, respectively). Compared with the present hydrogen beam injection systems, the ion heating ratio will increase in the deuterium beam injection systems in LHD owing to the increase in critical energy. The ion heating power is estimated to increase by 30% for the deuterium plasma and by 45% for the hydrogen plasma heated by deuterium beam injection. The ion and electron heating rates are summarized in Fig. 11 for various combinations of the target and beam species in the present hydrogen injection systems and planned deuterium injection systems.

Another advantage of the high-T_i operation in the deuterium experiment will be the reduction in the residual neutral density in the core, which should contribute to the development of the high-T_i discharge scenario. In addition, the confinement improvement owing to the isotope effect is also expected in the deuterium experiment. Therefore, 10 keV of the ion temperature will be achieved at the plasma density of 2×10^{19} m^{-3}.

7. Summary

Various heating scenarios to achieve high-T_i plasmas have been applied to the LHD experiments. The high-energy tangential negative-NBI, which was not available at the time of the designing LHD, was developed as the main approach to achieve high-performance plasmas, and has successfully extended the LHD parameter regime, especially for high-density and high-β plasmas. However, because the high-energy beams mainly heat the electrons, the ion temperature did not increase owing to insufficient ion heating power. To effectively increase the ion heating power, high-Z discharges with Ne and Ar were tried, and the increase in the ion temperature was confirmed with increasing ion heating power. As a result, 13.5 keV of the ion temperature was achieved with high-energy negative-NBIs. As the effectiveness of ion heating was confirmed for high-T_i plasmas in the high-Z discharges, low-energy perpendicular positive-NBIs were developed and installed to LHD for enhancing the ion heating power in hydrogen discharges. High-power heating with the positive-NBIs has resulted in increased ion temperature and extended the high-T_i plasma regime to more than 7 keV with the carbon pellet injection.

High-T_i plasmas are characterized by the ion ITB formation in which the ion transport is much improved by the reduction in the anomalous transport in the ion root with negative E_r. An impurity hole, in which impurities are released from the core, is observed in the ion ITB plasma. This property of high-T_i plasmas is conducive to reactor plasmas in which the impurity accumulation should be avoided. Repetitive long-pulse ICH helium main discharges are effective for wall conditioning to reduce the hydrogen recycling. Owing to the conditioning, the neutral density is reduced even in the core region and the density profile becomes peaked, leading to the enhancement of ion heating efficiency. Consequently, T_i of 7.5 keV has been achieved. The high-power ECRH is superposed to the high-T_i plasma, and high-performance plasmas with 6 keV of both ion and electron temperatures were obtained.

The deuterium experiment is planned in LHD as the next project step to extend the plasma performance to reactor-relevant parameters by improving the confinement owing to the isotope effect. In the deuterium beam heating, the ion heating power will increase and the ion temperature is expected to achieve a reactor-relevant 10 keV.

Acknowledgments

The authors acknowledge extensive contributions from overseas and domestic collaborators in the LHD high-T_i experiments. They are also grateful to the technical staff in the LHD for their excellent operation of the LHD system and the NBI, ECRH, and ICH systems. This study has been supported by a National Institute for Fusion Science grant for administrative budgets and partially supported by a Japan Society for the Promotion of Science Grant-in-Aid for Scientific Research.

[1] A. Iiyoshi *et al.*, Nucl. Fusion **39**, 1245 (1999).
[2] O. Motojima *et al.*, Phys. Plasmas **6**, 1843 (1999).
[3] A. Komori *et al.*, Fusion Sci. Technol. **58**, 1 (2010).
[4] Y. Takeiri *et al.*, Plasma Fusion Res. **3**, S1001 (2008).
[5] H. Yamada for the LHD Experiment Group, Nucl. Fusion **51**, 094021 (2011).
[6] O. Kaneko *et al.*, Nucl. Fusion **53**, 104015 (2013).
[7] T. Mutoh *et al.*, Nucl. Fusion **53**, 063017 (2013).
[8] O. Kaneko *et al.*, *Proc. 16th Int. Conf. Fusion Energy, Montreal, 1996, Vol. 3, International Atomic Energy Agency*, p. 539 (1997).
[9] Y. Takeiri *et al.*, J. Plasma Fusion Res. **74**, 1434 (1998).
[10] Y. Takeiri *et al.*, Rev. Sci. Instrum. **71**, 1225 (2000).
[11] O. Kaneko *et al.*, Nucl. Fusion **43**, 692 (2003).
[12] Y. Takeiri *et al.*, Nucl. Fusion **46**, S199 (2006).
[13] M. Osakabe *et al.*, *Proc. Joint 17th Int. Toki Conf. and 16th Int. Stellarator/Heliotron Workshop, Toki, Japan, 2007*, P2-079 (2007).
[14] Y. Takeiri *et al.*, Fusion Sci. Technol. **58**, 482 (2010).
[15] K. Nagaoka *et al.*, Plasma Fusion Res. **3**, S1013 (2008).
[16] K. Tsumori *et al.*, Fusion Sci. Technol. **58**, 489 (2010).
[17] T. Mutoh *et al.*, Phys. Rev. Lett. **85**, 4530 (2000).
[18] K. Saito *et al.*, Fusion Sci. Technol. **58**, 515 (2010).
[19] S. Murakami *et al.*, Nucl. Fusion **46**, S425 (2006).
[20] M. Yoshinuma *et al.*, Fusion Sci. Technol. **58**, 375 (2010).
[21] K.C. Shaing, Phys. Fluids **27**, 1567 (1984).
[22] T. Mutoh *et al.*, in Applications of Radio-Frequency Power to Plasmas, AIP Conference Proceedings **159**, 238 (1987).
[23] M. Yokoyama *et al.*, Contrib. Plasma Phys. **50**, 586 (2010).
[24] S. Morita, *et al.*, Nucl. Fusion **42**, 1179 (2002).
[25] Y. Takeiri *et al.*, Nucl. Fusion **45**, 565 (2005).
[26] T. Shimozuma *et al.*, Plasma Phys. Control. Fusion **45**, 1183 (2003).
[27] Y. Takeiri *et al.*, Phys. Plasmas **10**, 1788 (2003).
[28] Y. Takeiri *et al.*, Nucl. Fusion **47**, 1078 (2007).
[29] S. Morita, *et al.*, Nucl. Fusion **43**, 899 (2003).
[30] H. Takahashi *et al.*, Nucl. Fusion **53**, 073034 (2013).
[31] K. Nagaoka *et al.*, Proc. 25th International Atomic Energy Agency Fusion Energy Conference, St. Petersburg, 2014, PPC/2-1 (2014).
[32] M. Yokoyama *et al.*, Plasma Fusion Res. **7**, 2403011 (2012).
[33] M. Yokoyama *et al.*, Phys. Plasmas **15**, 056111 (2008).
[34] S. Matsuoka *et al.*, Plasma Fusion Res. **3**, S1056 (2008).
[35] K. Nagaoka *et al.*, Nucl. Fusion **51**, 083022 (2010).
[36] S. Murakami *et al.*, submitted to Plasma Phys. Control. Fusion.
[37] K. Ida *et al.*, Phys. Plasmas **16**, 056111 (2009).
[38] M. Yoshinuma *et al.*, Nucl. Fusion **49**, 062002 (2009).
[39] M. Yoshinuma *et al.*, *Proc. 23rd International Atomic Energy Agency Fusion Energy Conference, Daejon, 2010, EXC9-1* (2010).
[40] H. Takahashi *et al.*, submitted to Plasma Fusion Res.
[41] K. Fujii *et al.*, Rev. Sci. Instrum. **85**, 023502 (2014).
[42] Y. Takeiri *et al.*, *Joint 19th Int. Stellarator/Heliotron Workshop and 16th IEA-RFP Workshop, Padova, 2013*, B14 (2013).